

# Broadband waveguide quantum memory for entangled photons

Erhan Saglamyurek<sup>1</sup>, Neil Sinclair<sup>1</sup>, Jeongwan Jin<sup>1</sup>, Joshua A. Slater<sup>1</sup>, Daniel Oblak<sup>1</sup>, Félix Bussi eres<sup>1†</sup>, Mathew George<sup>2</sup>, Raimund Ricken<sup>2</sup>, Wolfgang Sohler<sup>2</sup> & Wolfgang Tittel<sup>1</sup>

**The reversible transfer of quantum states of light into and out of matter constitutes an important building block for future applications of quantum communication: it will allow the synchronization of quantum information<sup>1</sup>, and the construction of quantum repeaters<sup>2</sup> and quantum networks<sup>3</sup>. Much effort has been devoted to the development of such quantum memories<sup>1</sup>, the key property of which is the preservation of entanglement during storage. Here we report the reversible transfer of photon–photon entanglement into entanglement between a photon and a collective atomic excitation in a solid-state device. Towards this end, we employ a thulium-doped lithium niobate waveguide in conjunction with a photon-echo quantum memory protocol<sup>4</sup>, and increase the spectral acceptance from the current maximum<sup>5</sup> of 100 megahertz to 5 gigahertz. We assess the entanglement-preserving nature of our storage device through Bell inequality violations<sup>6</sup> and by comparing the amount of entanglement contained in the detected photon pairs before and after the reversible transfer. These measurements show, within statistical error, a perfect mapping process. Our broadband quantum memory complements the family of robust, integrated lithium niobate devices<sup>7</sup>. It simplifies frequency-matching of light with matter interfaces in advanced applications of quantum communication, bringing fully quantum-enabled networks a step closer.**

Quantum communication is founded on the encoding of information, generally referred to as quantum information, into quantum states of light<sup>6</sup>. The resulting applications of quantum physics at its fundamental level offer cryptographic security through quantum key distribution without relying on unproved mathematical assumptions<sup>8</sup> and allow for the disembodied transfer of quantum states between distant places by means of quantum teleportation<sup>6</sup>. Reversible mapping of quantum states between light and matter is central to advanced applications of quantum communication such as quantum repeaters<sup>2</sup> and quantum networks<sup>3</sup>, in which matter constitutes nodes that hold quantum information until needed, and thereby synchronize the information flow through the communication channel or network. Furthermore, such a quantum interface allows the generation of light–matter entanglement through the mapping of one of two entangled photons into matter. To determine whether and how different physical systems can be entangled, and to localize the fundamental or technological boundaries where this fascinating quantum link breaks down, are central goals in quantum physics and have received much attention over the past decades<sup>6</sup>.

The reversible light–matter interface can be realized through the direct transfer of quantum states from light onto matter and back, or through the generation of light–matter entanglement followed by teleportation of quantum information from an externally provided photon into matter, and eventually back. Experimental capabilities have advanced rapidly over the past years and quantum state transfer between light and atomic vapour<sup>9–13</sup>, solid-state ensembles<sup>4,14</sup>, or single absorbers<sup>15</sup>, as well as the generation of light–matter entanglement

through the absorption of photons<sup>16–18</sup>, or the emission of photons from atomic ensembles<sup>19–21</sup> or single emitters<sup>22,23</sup> have all been reported.

For quantum memory to become practical, it is important to reduce the complexity of experimental implementations, and the recent addition of rare-earth-ion-doped crystals<sup>4,14</sup> to the set of storage materials has been a valuable step towards this goal. The promise of such crystals is further enhanced through potentially long storage times—up to several seconds in Pr:Y<sub>2</sub>SiO<sub>5</sub> (ref. 24). In addition, given the large inhomogeneous broadening of optical zero-phonon lines, up to ~100-gigahertz (GHz), rare-earth-ion-doped crystals in principle offer storage of photons with less than 100-picosecond duration when being used in conjunction with a suitable quantum memory protocol<sup>4</sup>. Yet, the reversible state transfer between light and solid-state devices has so far not been shown to preserve entanglement. This is largely due to the limited spectral bandwidth of current implementations, 100 megahertz (MHz) at most<sup>5</sup>, which is orders of magnitude smaller than that of entangled photon pairs generated in the widely used process of spontaneous parametric down-conversion<sup>6</sup>. In this work, we approach the problem from both ends: we increase the acceptance bandwidth of our storage device to 5 GHz and narrow the bandwidths of our entangled photons to similar values. Furthermore, by using a wave-guiding storage medium, we move fundamental quantum memory research further towards application.

The layout of our experiment is depicted in Fig. 1. Short pulses of 523-nm wavelength light travel through an unbalanced interferometer. For sufficiently small pulse energies, subsequent spontaneous parametric down-conversion yields, to a good approximation, individual pairs of photons, centred at wavelengths around 795 nm and 1,532 nm, in the time-bin entangled qubit state<sup>25</sup>:

$$|\phi^+\rangle = \frac{1}{\sqrt{2}}(|e,e\rangle + |l,l\rangle) \quad (1)$$

Here,  $|e\rangle$  and  $|l\rangle$  denote early and late temporal modes and replace the usual spin-down and spin-up notation for spin-half particles. More specifically,  $|i,j\rangle$  denotes a quantum state in which the 795-nm photon has been created in the temporal mode  $i$ , and the 1,532-nm photon has been created in the temporal mode  $j$ . We point out that, owing to the spectral filtering, our source generates frequency-uncorrelated entangled photons at wavelengths that match the low-loss windows of free-space and standard telecommunication fibre. It can thus be readily used in real-world applications of quantum communication that involve quantum teleportation and entanglement swapping.

The 1,532-nm photon is directed to a qubit analyser. It consists of either a fibre delay line followed by a single-photon detector that monitors the photon's arrival time, or a fibre-optical interferometer that is unbalanced in the same way as the pump interferometer, followed by single-photon detectors. The role of the delay line is to perform projection measurements of the photon's state onto early and late qubit states. Alternatively, the interferometer enables projections onto

<sup>1</sup>Institute for Quantum Information Science, and Department of Physics and Astronomy, University of Calgary, 2500 University Drive NW, Calgary, Alberta. T2N 1N4, Canada. <sup>2</sup>Department of Physics—Applied Physics, University of Paderborn, Warburger Strasse 100, 33095 Paderborn, Germany. <sup>†</sup>Present address: GAP-Optique, University of Geneva, Rue de l' cole-de-M decine 20, 1211 Geneva 4, Switzerland.

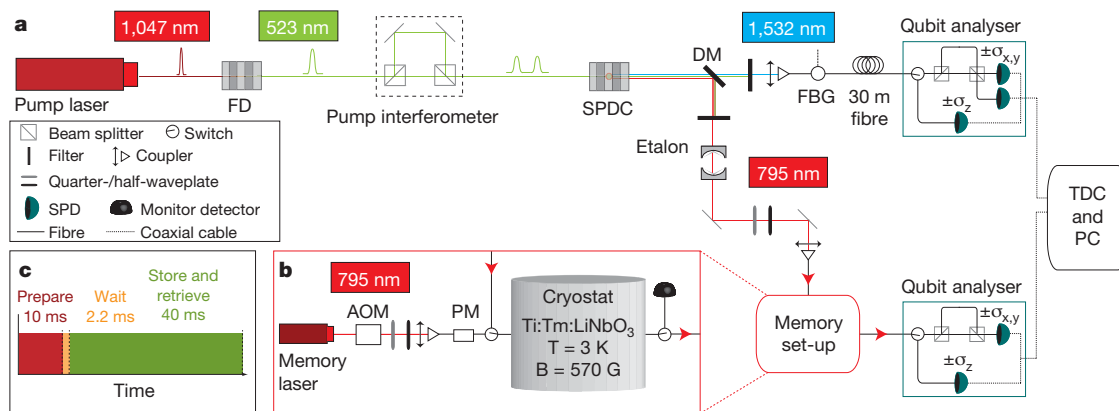


**Figure 1 | Schematics of the experimental set-up.** **a**, Generating and measuring entanglement. Six-picosecond-long pump laser pulses (1,047.328 nm wavelength, 80 MHz repetition rate) are frequency doubled (FD) in a periodically poled lithium niobate (PPLN) crystal. Each resulting 16-ps-long pulse (523.664 nm wavelength, 90 mW average power) is coherently split into two by the unbalanced pump interferometer, featuring a 1.4-ns time-time difference. Spontaneous parametric down-conversion (SPDC) in a second PPLN crystal followed by frequency filtering using an etalon and a fibre Bragg grating (FBG) (bandwidths of 6 GHz and 9 GHz, respectively), yields maximally entangled pairs of photons centred at 795.506 nm and 1,532.426 nm wavelength (DM, dichroic mirror). The 1,532-nm photon travels through a 30-m telecommunication fibre, and the 795-nm photon is either stored in the memory or sent through a fibre delay line (not pictured). To characterize the biphoton state, we use qubit analysers consisting of delay lines or unbalanced interferometers connected to single-photon detectors. Detection events are

equal superpositions of early and late modes<sup>25</sup>. Using the language of spin-half systems, this corresponds to projections onto  $\sigma_z$  and, for appropriately chosen phases,  $\sigma_x$  and  $\sigma_y$ , respectively.

The 795-nm photon is transmitted to the quantum memory where its state—specifically that it is entangled with the 1,532-nm photon—is mapped onto a collective excitation of millions of thulium ions. Some time later, the state is mapped back onto a photon that exits the memory through a fibre in well-defined spatio-temporal modes and is probed by a second qubit analyser.

collected with a time-to-digital converter (TDC) connected to a personal computer (PC). All interferometers are phase-locked to stable reference lasers (not shown). **b**, Memory set-up. The 795.506-nm continuous-wave memory laser beam is intensity- and phase/frequency-modulated using an acousto-optic modulator (AOM) and a phase modulator (PM). The waveguide is cooled to 3 K and exposed to a 570-G magnetic field aligned with the crystal's  $C_3$ -axis. Waveplates allow adjusting the polarization of the beam to the waveguide's transverse magnetic (TM) mode, and optical switches combine and separate the optical pump beam and the 795-nm photons. **c**, Timing sequence. We use three continuously repeated phases: the 10 ms 'prepare' phase for optical pumping, the 2.2-ms 'wait' phase, which ensures stored photons are not polluted by fluorescence from the excited state, and the 40-ms 'store and retrieve' phase, during which many 795-nm photons are successively stored in the waveguide and recalled after 7 ns.

To reversibly map the 795-nm photon onto matter, we use a photon-echo quantum memory protocol based on atomic frequency combs (AFC)<sup>4</sup>. It is rooted in the interaction of light with an ensemble of atomic absorbers (so far rare-earth-ion-doped crystals cooled to cryogenic temperatures) with an inhomogeneously broadened absorption line that has been tailored into a series of equally spaced absorption peaks (see Fig. 2). The absorption of a single photon leads to a collective excitation shared by many atoms. Owing to the particular shape of the tailored absorption line, the excited collective coherence rapidly dephases and repeatedly recovers after multiples of the storage time  $T_s$ . This results in the re-emission of a photon in the state encoded into the original photon.

In our implementation the moment of photon re-emission is pre-determined by the spacing of the teeth in the comb,  $T_s = 1/\Delta$ , and the storage process can be described as arising from the linear response of an optical filter made by spectral hole burning. Yet, readout on demand can be achieved by temporarily mapping the optically excited coherence onto ground-state coherence where the comb spacing is smaller or the comb structure is washed out<sup>4</sup>, or by combining the AFC protocol with controlled reversible inhomogeneous broadening of each absorption line, similar to the storage mechanism used in another photon-echo quantum memory protocol<sup>1</sup>.

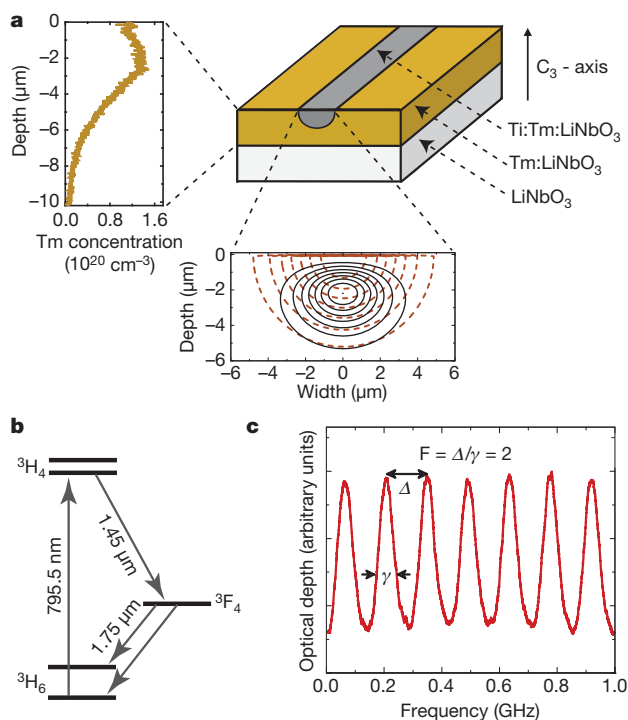


**Figure 2 | The storage medium.** **a**, Waveguide geometry. The measured thulium (Tm) concentration profile is given on the left and the calculated intensity distribution of the fundamental TM-mode at the 795-nm wavelength is shown below. Iso-intensity lines are plotted corresponding to 100%, 87.5%, 75% and so on of the maximum intensity. **b**, Simplified energy level diagram of thulium ions. The optical coherence time of the  ${}^3\text{H}_6 \leftrightarrow {}^3\text{H}_4$  transition at 3 K is 1.6  $\mu\text{s}$ , the radiative lifetimes of the  ${}^3\text{H}_4$  and  ${}^3\text{F}_4$  levels are 82  $\mu\text{s}$  and 2.4 ms, respectively, and the branching ratio from the  ${}^3\text{H}_4$  to the  ${}^3\text{F}_4$  level is 44%. Upon application of a magnetic field of 570 G, the ground and excited levels split into magnetic sublevels with lifetimes exceeding one second<sup>27</sup>. **c**, Atomic frequency comb. The bandwidth of our AFC is 5 GHz (shown here is a 1-GHz broad section). The separation between the teeth is  $\Delta \approx 143$  MHz, resulting in 7 ns storage time. The line width of the peaks is  $\gamma \approx 75$  MHz, yielding a finesse  $F = 2$ , as expected for the sinus-type comb.

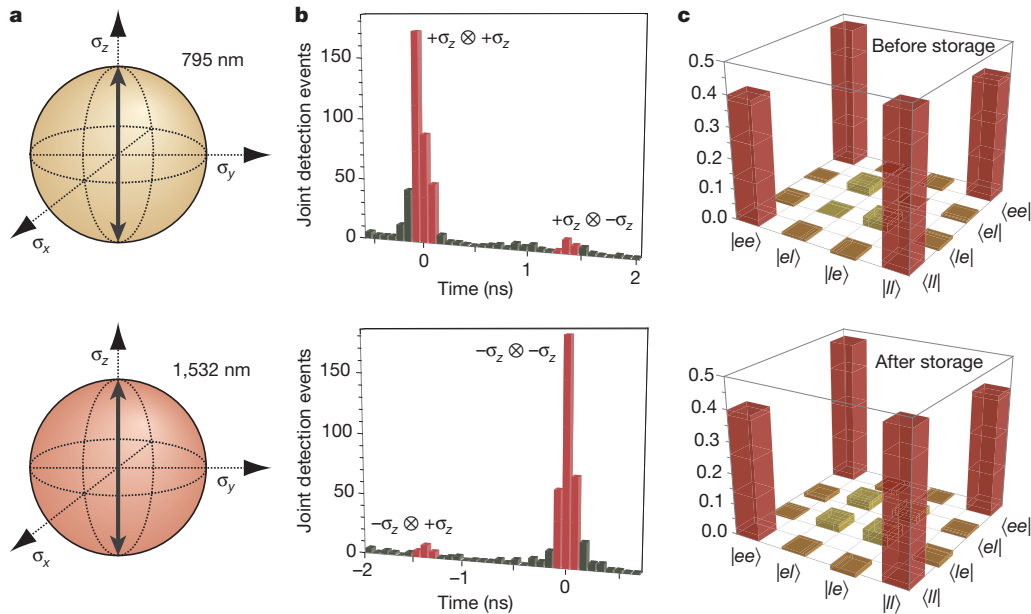


**Figure 3 | Measurement of density matrices.** **a**, Visualization of projection measurements. The measurement settings for the 795-nm (or 1,532-nm) qubit analyser are depicted on the upper (or lower) Bloch sphere. The example shows joint settings that enable calculating normalized probabilities for projections onto  $\sigma_z \otimes \sigma_z$  and  $\sigma_z \otimes -\sigma_z$ . **b**, Results for joint projection measurement after storage. The top (bottom) histogram displays joint detection events for the projection onto  $\sigma_z \otimes \sigma_z$  and  $\sigma_z \otimes -\sigma_z$  ( $-\sigma_z \otimes \sigma_z$  and  $-\sigma_z \otimes -\sigma_z$ ) as a function of the time difference between detections of the 795-nm and the 1,532-nm

photons. The desired events are those within the red-highlighted time windows. This allows us to calculate the joint-detection probabilities for projections onto  $\sigma_z \otimes \sigma_z$  and  $\sigma_z \otimes -\sigma_z$  (for results with other joint settings see the Supplementary Information). **c**, Density matrices. Density matrices were calculated using a maximum-likelihood estimation for the bi-photon states before and after storage. Only the real parts are shown—the absolute values of all imaginary components are below 0.04.

Our storage device, a Ti:Tm:LiNbO<sub>3</sub> optical waveguide cooled to 3 K, is detailed in Fig. 2. It was previously characterized to establish its suitability as a photon-echo quantum memory material<sup>26</sup>. It combines interesting properties from the specific rare-earth element (795-nm storage wavelength), the host crystal (allowing for controlled dephasing and rephasing by means of electric fields), and from the waveguiding structure (ease-of-use). Lithium niobate waveguides have also been doped with neodymium, praseodymium and erbium<sup>7</sup>, and we conjecture that other rare-earth ions could also be used. This could extend the properties of LiNbO<sub>3</sub> and allow an integrated approach to other storage wavelengths, ions with different level structures, and so on.

To generate the AFC, we use a sideband-chirping technique (see Supplementary Information) to transfer atomic population between magnetic sublevels and create troughs and peaks in the inhomogeneously broadened absorption line. They form a 5-GHz-wide comb with tooth spacing of 143 MHz, setting the storage time to 7 ns. The system efficiency in our implementation is currently about 0.2%. This is in part due to the 90% fibre-to-waveguide input and output coupling loss, which we attribute to imperfect mode overlap. In addition, owing to the specific level structure of thulium under current experimental conditions, the finesse of the comb in the broadband approach is two, which limits the memory efficiency to about 10%. However, imperfections in the creation of the comb decrease this efficiency to around 2%. The system efficiency can be increased by improving the spectral tailoring of the AFC, and triggering photon re-emission in the backward direction. By also optimizing the mode overlap, we anticipate that it could reach

approximately 15%. Furthermore, if the two long-lived atomic levels between which population is transferred during the optical pumping procedure (in our case the two magnetic ground states; see Fig. 2) are spaced by more than the storage bandwidth, the memory efficiency can theoretically reach unity (see Supplementary Information).

To assess the quantum nature of our light–matter interface, we first make projection measurements with the 795-nm photons and the 1,532-nm photons onto time-bin qubit states characterized by Bloch vectors aligned along **a** and **b**, respectively, where **a**, **b**  $\in$  [ $\pm\sigma_x, \pm\sigma_y, \pm\sigma_z$ ] (see Fig. 3). Experimentally, this is done by means of suitably adjusted qubit analysers, and by counting the number  $C(\mathbf{a}, \mathbf{b})$  of detected photon pairs. From two such spin-measurements, we calculate the normalized joint-detection probability:

$$P(\mathbf{a}, \mathbf{b}) = \frac{C(\mathbf{a}, \mathbf{b})}{C(\mathbf{a}, \mathbf{b}) + C(\mathbf{a}, -\mathbf{b})} \quad (2)$$

The measurement and the results with the fibre delay line, as well as the memory, are detailed in Fig. 3 and the Supplementary Information. From this data, we reconstruct the bi-photon states before and after storage in terms of their density matrices  $\rho_{\text{in}}$  and  $\rho_{\text{out}}$ , depicted in Fig. 3, using a maximum likelihood estimation<sup>27</sup>. This, in turn, allows us to examine the entanglement of formation<sup>28</sup>, a measure that indicates entanglement if it exceeds zero; it is upper-bounded by one. The results, listed in Table 1, clearly show the presence of entanglement in  $\rho_{\text{in}}$  and  $\rho_{\text{out}}$  and, within experimental uncertainty, establish that the storage process preserves entanglement without measurable degradation.

**Table 1 | Entanglement measures, purities and fidelities**

	Entanglement of formation (%)	Purity (%)	Fidelity with $ \phi^+\rangle$ (%)	Input/output fidelity (%)	Expected $S_{\text{th}}$	Measured $S$
$\rho_{\text{in}}$	64.4 $\pm$ 4.2	75.7 $\pm$ 2.4	86.2 $\pm$ 1.5		2.235 $\pm$ 0.085	2.379 $\pm$ 0.034
$\rho_{\text{out}}$	65 $\pm$ 11	76.3 $\pm$ 5.9	86.6 $\pm$ 3.9	95.4 $\pm$ 2.9	2.2 $\pm$ 0.22	2.25 $\pm$ 0.06

Entanglement of formation (normalized with respect to the entanglement of formation of  $|\phi^+\rangle$ ), purity  $P = \text{tr}(\rho^2)$ , fidelity with  $|\phi^+\rangle$ , input–output fidelity  $F = (\text{tr}(\sqrt{\sqrt{\rho_{\text{out}}}\rho_{\text{in}}\sqrt{\rho_{\text{out}}}}))^2$  (referring to the fidelity of  $\rho_{\text{out}}$  with respect to  $\rho_{\text{in}}$ ), and expected and experimentally obtained  $S$  values for tests of the CHSH Bell inequality (measured for  $\mathbf{a} = \sigma_x, \mathbf{a}' = \sigma_y, \mathbf{b} = \sigma_x + \sigma_y$ , and  $\mathbf{b}' = \sigma_x - \sigma_y$ ). The correlation coefficients used to compute  $S$  and the calculation of  $S_{\text{th}}$  are detailed in the Supplementary Information. We note that the original state (and hence the recalled state) has limited purity and fidelity with  $|\phi^+\rangle$ . This is due to the probabilistic nature of our spontaneous parametric down-conversion source, which features a non-negligible probability of generating more than two photons simultaneously<sup>26</sup>. Uncertainties indicate one-sigma standard deviations and are estimated from Poissonian detection statistics and using a Monte Carlo simulation.

Furthermore, we note that the fidelity  $F$  between  $\rho_{\text{in}}$  and  $\rho_{\text{out}}$  is close to one, and hence the unitary transformation introduced by the storage process is almost the identity transformation.

In addition, as a second entanglement measure, we perform tests of the Clauser–Horne–Shimony–Holt (CHSH) Bell inequality<sup>6</sup>. This test indicates non-local correlations and thus the possibility of using the bi-photons for entanglement-based quantum key distribution<sup>8</sup> if the sum:

$$S = |E(\mathbf{a}, \mathbf{b}) + E(\mathbf{a}', \mathbf{b}) + E(\mathbf{a}, \mathbf{b}') - E(\mathbf{a}', \mathbf{b}')| \quad (3)$$

of four correlation coefficients

$$E(\mathbf{a}, \mathbf{b}) = \frac{C(\mathbf{a}, \mathbf{b}) - C(\mathbf{a}, -\mathbf{b}) - C(-\mathbf{a}, \mathbf{b}) + C(-\mathbf{a}, -\mathbf{b})}{C(\mathbf{a}, \mathbf{b}) + C(\mathbf{a}, -\mathbf{b}) + C(-\mathbf{a}, \mathbf{b}) + C(-\mathbf{a}, -\mathbf{b})} \quad (4)$$

with appropriately chosen settings  $\mathbf{a}, \mathbf{a}'$  and  $\mathbf{b}, \mathbf{b}'$  exceeds the classical bound of two; quantum mechanically it is upper-bounded by  $2\sqrt{2}$ . As detailed in Table 1, we find  $S_{\text{in}} = 2.379 \pm 0.034 > 2$  before the memory and, crucially,  $S_{\text{out}} = 2.25 \pm 0.06 > 2$ , which is in agreement with the value  $S_{\text{th}} = 2.2 \pm 0.22$  predicted from the reconstructed density matrix  $\rho_{\text{out}}$ . This validates the suitability of our set-up for quantum communication.

Our investigation provides an example of entanglement being transferred between physical systems of different nature, thereby adding evidence that this fundamental quantum property is not as fragile as is often believed. Furthermore, our broadband integrated approach permits the linkage of a promising quantum storage device with extensively used, high-performance sources of photons in bi- and multipartite entangled states<sup>6</sup>. Although the storage efficiency and the storage time need to be significantly increased, and the moment of recall was pre-set, this study opens the way to new investigations of fundamental and applied aspects of quantum physics. Having increased the storage bandwidth also significantly facilitates the building of future quantum networks, because mutual frequency matching of photons and distant quantum memories will be simple. In addition, a large storage bandwidth—that is, the possibility to encode quantum information into short optical pulses—allows us to increase the number of temporal modes that can be stored during a given time. This enhances the flow of quantum information through a network and decreases the time needed to establish entanglement over a large distance using a quantum repeater<sup>1,2</sup>.

We note that, parallel to this work, Clausen *et al.* have demonstrated the storage of an entangled photon using a neodymium-doped crystal<sup>29</sup>.

Received 1 September; accepted 6 December 2010.

Published online 12 January 2011.

1. Lvovsky, A. I., Sanders, B. C., & Tittel, W. Optical quantum memory. *Nature Photon.* **3**, 706–714 (2009).
2. Sangouard, N., Simon, C., de Riedmatten, H. & Gisin, N. Quantum repeaters based on atomic ensembles and linear optics. Preprint at (<http://arxiv.org/abs/0906.2699>) (2009).
3. Kimble, H. J. The quantum Internet. *Nature* **453**, 1023–1030 (2008).
4. de Riedmatten, H., Afzelius, M., Staudt, M. U., Simon, C. & Gisin, N. A solid-state light–matter interface at the single-photon level. *Nature* **456**, 773–777 (2008).
5. Usmani, I., Afzelius, M., de Riedmatten, H. & Gisin, N. Mapping multiple photonic qubits into and out of one solid-state atomic ensemble. *Nature Commun.* **1**, 1–7 (2010).
6. Pan, J.-W., Chen, Z.-B., Żukowski, M., Weinfurter, H. & Zeilinger, A. Multi-photon entanglement and interferometry. Preprint at (<http://arxiv.org/abs/0805.2853>) (2008).

7. Sohler, W. *et al.* Integrated optical devices in lithium niobate. *Opt. Photon. News* 24–31 (January 2008).
8. Gisin, N., Ribordy, G., Tittel, W. & Zbinden, H. Quantum cryptography. *Rev. Mod. Phys.* **74**, 145–195 (2002).
9. Julsgaard, B., Sherson, J. & Cirac, J. I. J. Fűrášek, J. & Polzik, E. S. Experimental demonstration of quantum memory for light. *Nature* **432**, 482–486 (2004).
10. Chanelière, T. *et al.* Storage and retrieval of single photons transmitted between remote quantum memories. *Nature* **438**, 833–836 (2005).
11. Eisaman, M. D. *et al.* Electromagnetically induced transparency with tunable single-photon pulses. *Nature* **438**, 837–841 (2005).
12. Honda, K. *et al.* Storage and retrieval of a squeezed vacuum. *Phys. Rev. Lett.* **100**, 093601 (2008).
13. Appel, J., Figueroa, E., Korystov, D., Lobino, M. & Lvovsky, A. Quantum memory for squeezed light. *Phys. Rev. Lett.* **100**, 093602 (2008).
14. Hedges, M. P., Longdell, J. J., Li, Y. & Sellars, M. J. Efficient quantum memory for light. *Nature* **465**, 1052–1056 (2010).
15. Boozer, A. D. *et al.* Reversible state transfer between light and a single trapped atom. *Phys. Rev. Lett.* **98**, 193601 (2007).
16. Choi, C. S. & Deng, H. Laurat, J. & Kimble, H. J. Mapping photonic entanglement into and out of a quantum memory. *Nature* **452**, 67–71 (2008).
17. Akiba, K. & Kashiwagi, K. Arikawa, M. & Kozuma, M. Storage and retrieval of non-classical photon pairs and conditional single photons generated by the parametric down-conversion process. *N. J. Phys.* **11**, 013049 (2009).
18. Jin, X.-M. *et al.* Quantum interface between frequency-uncorrelated down-converted entanglement and atomic-ensemble quantum memory. Preprint at (<http://arxiv.org/abs/1004.4691>) (2010).
19. Chou, C. W. *et al.* Measurement-induced entanglement for excitation stored in remote atomic ensembles. *Nature* **438**, 828–832 (2005).
20. Matsukevich, D. N. *et al.* Entanglement of a photon and a collective atomic excitation. *Phys. Rev. Lett.* **95**, 040405 (2005).
21. Yuan, Z.-S. *et al.* Experimental demonstration of a BDCZ quantum repeater node. *Nature* **454**, 1098–1101 (2008).
22. Blinov, B. B., Moehring, D. L., Duan, L.-M. & Monroe, C. Observation of entanglement between a single trapped atom and a single photon. *Nature* **428**, 153–157 (2004).
23. Togan, E. *et al.* Quantum entanglement between an optical photon and a solid-state spin qubit. *Nature* **466**, 730–734 (2010).
24. Longdell, J., Fraval, E., Sellars, M. & Manson, N. Stopped light with storage times greater than one second using electromagnetically induced transparency in a solid. *Phys. Rev. Lett.* **95**, 063601 (2005).
25. Marcikic, I. *et al.* Time-bin entangled qubits for quantum communication created by femtosecond pulses. *Phys. Rev. A* **66**, 062308 (2002).
26. Sinclair, N. *et al.* Spectroscopic investigations of a Ti:TM:LiNbO<sub>3</sub> waveguide for photon-echo quantum memory. *J. Lumin.* **130**, 1586–1593 (2010).
27. Altepeter, J. B., Jeffrey, E. R., & Kwiat, P. G. Photonic state tomography. *Adv. At. Mol. Opt. Phys.* **52**, 105–159 (2005).
28. Plenio, M. B. & Virmani, S. An introduction to entanglement measures. *Quant. Inf. Comput.* **7**, 1–51 (2007).
29. Clausen, C. *et al.* Quantum storage of photonic entanglement in a crystal. *Nature* doi:10.1038/nature09662 (this issue).

Supplementary Information is linked to the online version of the paper at [www.nature.com/nature](http://www.nature.com/nature).

**Acknowledgements** This work is supported by NSERC, QuantumWorks, General Dynamics Canada, iCORE (now part of Alberta Innovates), CFI, AAET and FQRNT. We thank C. La Mela, T. Chanelière, T. Stuart, V. Kiselyov and C. Dascalos for help during various stages of the experiment, C. Simon, K. Rupavatharam and N. Gisin for discussions, and A. Lvovsky for lending us a single-photon detector.

**Author Contributions** The Ti:TM:LiNbO<sub>3</sub> waveguide was fabricated and characterized at room temperature by M.G., R.R. and W.S. The photon-pair source was built by J.J., J.A.S. and F.B., the AFC memory set-up was developed by E.S. and N.S., and the complete experiment was conceived and directed by W.T. The measurements and the analysis were done by E.S., N.S., J.J., J.A.S., D.O. and W.T., and W.T., E.S., N.S., J.J., J.A.S. and D.O. wrote the paper. E.S., N.S., J.J. and J.A.S. contributed equally to this work.

**Author Information** Reprints and permissions information is available at [www.nature.com/reprints](http://www.nature.com/reprints). The authors declare no competing financial interests. Readers are welcome to comment on the online version of this article at [www.nature.com/nature](http://www.nature.com/nature). Correspondence and requests for materials should be addressed to W.T. ([wtittel@ucalgary.ca](mailto:wtittel@ucalgary.ca)).

Copyright of Nature is the property of Nature Publishing Group and its content may not be copied or emailed to multiple sites or posted to a listserv without the copyright holder's express written permission. However, users may print, download, or email articles for individual use.